

Second-Generation Dual FXR/sEH Modulators with Optimized Pharmacokinetics

Moritz Helmstädter, Astrid Kaiser, Steffen Brunst, Jurema Schmidt, Riccardo Ronchetti, Lilia Weizel, Ewgenij Proschak, and Daniel Merk*

Cite This: *J. Med. Chem.* 2021, 64, 9525–9536

Read Online

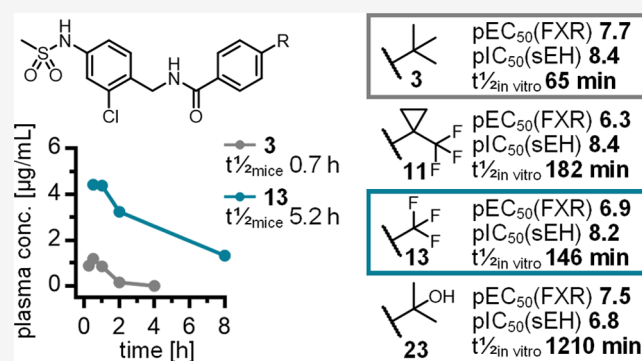
ACCESS |

Metrics & More

Article Recommendations

Supporting Information

ABSTRACT: Non-alcoholic steatohepatitis (NASH) presents as an epidemic chronic liver disease that is closely associated with metabolic disorders and involves hepatic steatosis, inflammation, and fibrosis as key factors. Despite the enormous global prevalence of NASH, effective pharmacological interventions are lacking. Based on the hypothesis that the multifactorial condition NASH may benefit from combined multiple modes of action for enhanced therapeutic efficacy, we have previously developed dual FXR activators/sEH inhibitors (FXRa/sEHi) and observed remarkable antifibrotic effects upon their use in rodent NASH models. However, these first-generation FXRa/sEHi were characterized by moderate metabolic stability and short in vivo half-life. Aiming to overcome these pharmacokinetic drawbacks, we have systematically studied the structure–activity and structure–stability relationships of the chemotype and obtained second-generation FXRa/sEHi with improved pharmacokinetic parameters. With high plasma exposure, a half-life greater than 5 h, and similar dual potency on the intended targets, **13** presents as a substantially optimized FXRa/sEHi for late-stage preclinical development.

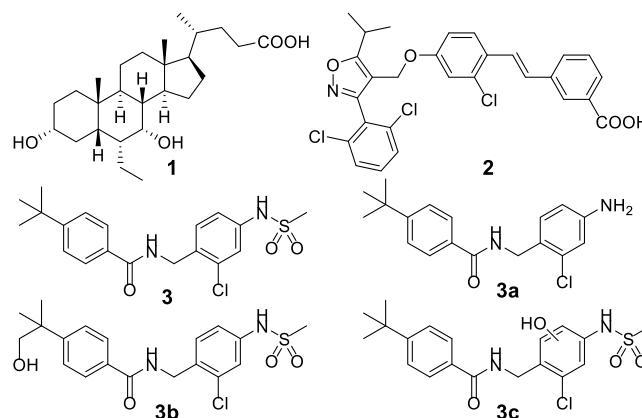


INTRODUCTION

Despite enormous global efforts to develop effective pharmacological treatments for non-alcoholic steatohepatitis (NASH), there is still no drug available to counter this severe chronic liver disorder.¹ NASH, which mainly arises from overnutrition and unhealthy lifestyle, is characterized by a triad of hepatic pathologies, namely steatosis, inflammation, and fibrosis in liver.^{2–5} As hepatic manifestation of the metabolic syndrome, the complex of non-alcoholic fatty liver disease (NAFLD)/NASH has an alarming global prevalence and can progress to liver cirrhosis and hepatocellular carcinoma as potentially lethal consequences.^{1,4,5} Effective therapeutic interventions for this pathology are, hence, urgently needed. There are a number of drugs in late-stage clinical development to treat NASH¹ with the farnesoid X receptor (FXR) agonist obeticholic acid⁶ (OCA, **1**) as a frontrunner (Chart 1) despite recent drawbacks.⁷ In addition, a number of descendants of the widely used FXR agonist GW4064 (**2**)⁸ follow in earlier stages of clinical trials.¹ Although FXR agonists had promising efficacy in phase 2 trials,^{9,10} however, no approval has been granted yet.

As outlined above, NASH is a highly multifactorial disease. Designed polypharmacology¹¹ has therefore been proposed as a potentially superior approach to treat NASH. By simultaneously addressing multiple therapeutic modes of action, designed multitarget agents may achieve additive or even synergistic efficacy. In an attempt to establish such a

Chart 1. FXR agonists OCA (**1**) and GW4064 (**2**), Dual FXR Agonist/sEH Inhibitor **3** and Its Metabolites **3a–c**



Received: May 7, 2021
Published: June 24, 2021



concept for experimental NASH treatment, we have previously developed a potent and balanced dual FXR agonist and soluble epoxide hydrolase (sEH) inhibitor (FXRa/sEHi).¹²

These two modes of action were chosen for the polypharmacological approach based on preclinical and clinical observations on their individual therapeutic potential in NASH and their complementary effects. FXR is a liver-protective transcription factor, and its activation has been shown to exhibit pronounced antisteatotic and some anti-inflammatory effects.^{9,13–15} Inhibition of the sEH appeared very suitable to complement these therapeutic effects of FXR activation for its well-documented anti-inflammatory,^{16–18} antifibrotic,^{17–19} and antiapoptotic²⁰ properties. The sEH is a downstream enzyme of the cytochrome P450 (CYP) epoxygenase pathway and degrades epoxyeicosatrienoic acids (EET) to the corresponding diols.²¹ Inhibition of the sEH leading to increased EET levels proved beneficial for the treatment of various inflammatory diseases and has shown efficacy in rodent models of NASH.^{16,19,22–26} Indeed, our dual FXRa/sEHi **3**¹² has demonstrated promising anti-NASH effects in three preclinical models of the disease as preventive²⁷ and curative²⁸ intervention. Therein, **3** especially revealed pronounced antifibrotic activities,^{27,28} which is particularly attractive since fibrosis is considered a major prognostic factor of NASH progression.^{4,5}

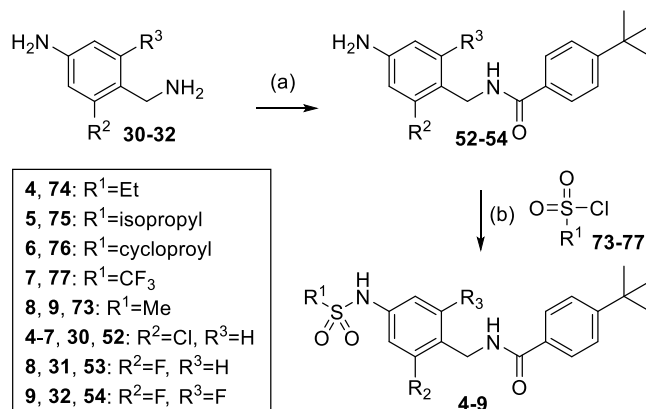
The FXRa/sEHi **3** was obtained by rational design of a minimal dual pharmacophore and subsequent structural optimization.¹² It comprises a designed dual activity profile with high potency on FXR (pEC₅₀ 7.7) and sEH (pIC₅₀ 8.4) but has pharmacokinetic liabilities due to moderate metabolic stability resulting in a half-life below 1 h. By LC-MS analysis, we found that metabolic conversion of **3** mainly leads to the metabolites **3a–c** via sulfonamide hydrolysis and hydroxylation (Chart 1).¹² Since the efficacy of **3** in various rodent models of NASH and other fibrotic diseases has confirmed great therapeutic potential of dual FXR/sEH modulation, we aimed to overcome the pharmacokinetic limitations of **3** and generate a second-generation derivative with improved metabolic stability while retaining dual potency. To achieve this objective, we have systematically elucidated the structure–activity and structure–stability relationships of the FXRa/sEHi chemotype and focused on incorporating modifications with the potential to stabilize or replace the metabolic soft spots. In particular, we probed metabolic stabilization of the sulfonamide and the oxidation-sensitive tert-butyl moiety with sterically demanding electron-withdrawing and bioisosteric groups. This challenging multi-objective optimization yielded a second-generation FXRa/sEHi with substantially improved pharmacokinetics as intended.

RESULTS AND DISCUSSION

Chemistry. Second-generation derivatives **4–29** of the FXRa/sEHi chemotype **3** were prepared according to Schemes 1–8. Benzylamines **30–32** and benzoic acid derivatives **33–51** served as building blocks for the synthesis of benzamides **52–72** using EDC·HCl and 4-DMAP as coupling agents for amide bond formation. Benzamides **52–72** were then reacted with sulfonyl chlorides **73–77** in the presence of pyridine to yield second-generation derivatives **4–9** (Scheme 1), **11–24**, and **26–29** (Scheme 2).

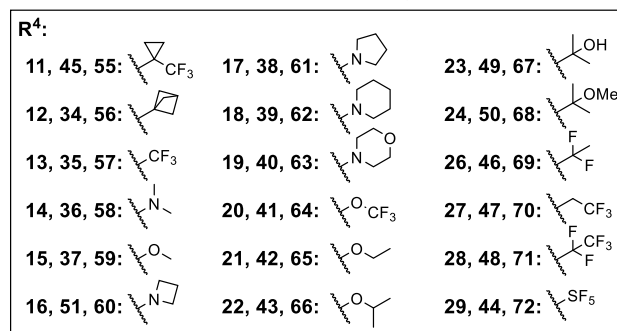
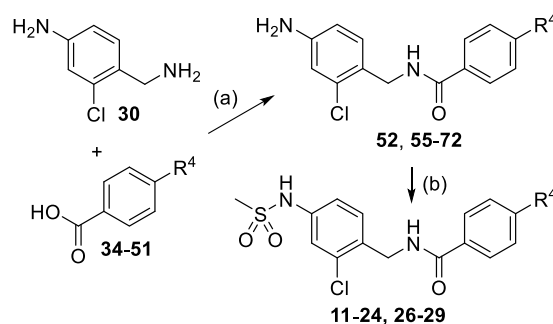
The required anilines **30–32** were obtained by reduction of commercially available benzonitriles **78–80** with LiAlH₄ (Scheme 3). Benzoic acid precursors **33–44** were commer-

Scheme 1. Synthesis of 4–9^a



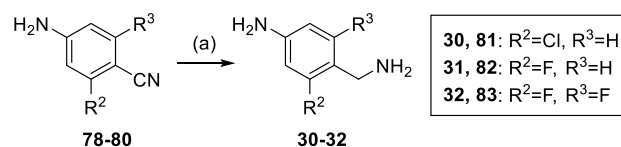
^aReagents and conditions: (a) 4-*tert*-butylbenzoic acid (**33**), EDC·HCl, 4-DMAP, CHCl₃, 50 °C, 16 h, yield: 16–66%; and (b) tetrahydrofuran (THF), pyridine, 0–66 °C, 2–16 h, yield: 15–60%.

Scheme 2. Synthesis of 11–24 and 26–29^a



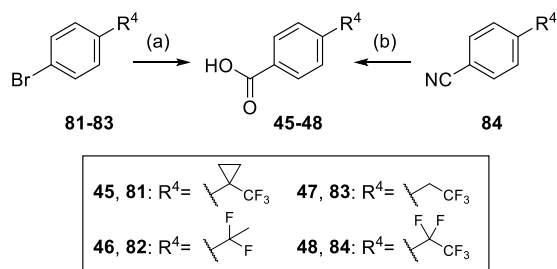
^aReagents and conditions: (a) EDC·HCl, 4-DMAP, CHCl₃, 50 °C, 16 h, yield: 10–87%; and (b) THF, mesyl chloride (**73**), pyridine, reflux, 2–16 h, yield: 5–69%.

Scheme 3. Synthesis of Aniline Precursors 30–32^a



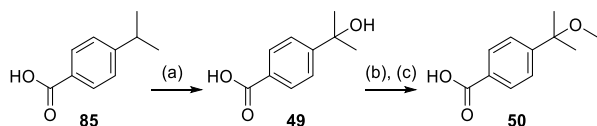
^aReagents and conditions: (a) LiAlH₄, THF, rt, 18 h, yield: 60–75%.

cially available, and **45–47** were synthesized in a palladium-catalyzed hydroxycarbonylation reaction adapted from Wu et al.²⁹ using aryl bromides **81–83**, Pd(OAc)₂, XantPhos, EDC·HCl, triethylamine, and formic acid. Benzoic acid derivative **48** was accessible via hydrolysis of benzonitrile **84** using KOH (Scheme 4).

Scheme 4. Synthesis of Benzoic Acid Precursors 45–48^a

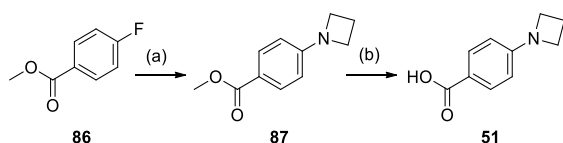
^aReagents and conditions: (a) Pd(OAc)₂, XantPhos, EDC·HCl, NEt₃, formic acid, DMF, 50 °C, 20 h, yield: 48–79%; and (b) KOH, H₂O, EtOH, reflux, 48 h, yield: 36%.

Oxidation of 4-isopropylbenzoic acid (**85**) using KMnO₄ in the presence of pyridine yielded benzoic acid derivative **49**, which subsequently served as a precursor for the synthesis of benzoic acid derivative **50** using H₂SO₄/MeOH and LiOH/H₂O/MeOH in a two-step procedure (Scheme 5).

Scheme 5. Synthesis of Benzoic Acid Precursors 49 and 50^a

^aReagents and conditions: (a) KMnO₄, H₂O, pyridine, reflux, 17 h, yield: 46%; (b) H₂SO₄, MeOH, 80 °C, 2 h; and (c) LiOH, H₂O, MeOH, THF, 3 h, yield: 82%.

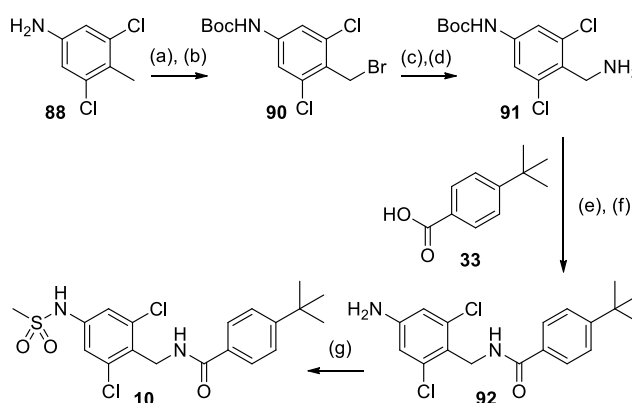
The benzoic acid precursor **51** was prepared in a nucleophilic aromatic substitution of methyl 4-fluorobenzoate (**86**) using azetidine hydrochloride, followed by a hydrolysis of the methylester in **87** to **51** (Scheme 6).

Scheme 6. Synthesis of Precursor 51^a

^aReagents and conditions: (a) azetidine hydrochloride, K₂CO₃, DMSO, reflux, 72 h; and (b) LiOH, H₂O, EtOH, 16 h, yield: 42% over two steps.

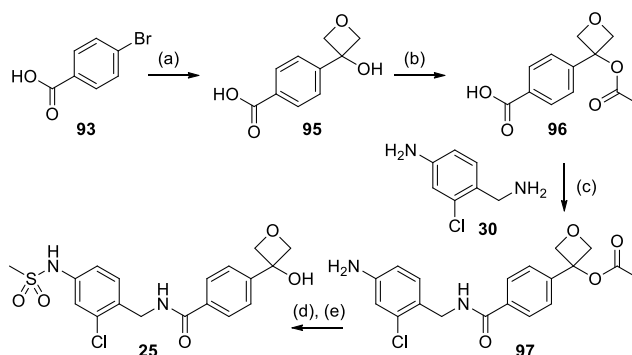
The second-generation FXRa/sEH candidates **10** and **25** were not accessible via the general route outlined in Scheme 1 and had to be synthesized using protecting groups. Di-*tert*-butyl dicarbonate enabled the protection of 3,5-dichloro-4-methylaniline (**88**), which was then used for the synthesis of **90** by radical bromination. A two-step Staudinger reaction using sodium azide and triphenylphosphine yielded the Boc-protected aminomethylaniline **91**, which was further reacted to the respective *tert*-butylbenzamide **92** using 4-*tert*-butylbenzoic acid (**33**), EDC·HCl, and 4-DMAP and subsequent Boc-cleavage with trifluoroacetic acid. Mesylation of **92** using mesylchloride (**73**) and pyridine then afforded **10** (Scheme 7).

A lithium halogen exchange using *n*-BuLi and 4-bromobenzoic acid (**93**) followed by a reaction with 3-oxetanone (**94**) in a two-step procedure yielded benzoic acid

Scheme 7. Synthesis of 10^a

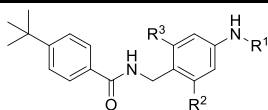
^aReagents and conditions: (a) di-*tert*-butyl dicarbonate, THF, 60 °C, yield: 83%; (b) NBS, AIBN, CHCl₃, reflux, 4 h, yield: 77%; (c) NaN₃, DMF, 80 °C, 16 h; (d) PPh₃, H₂O, THF, rt, 12 h, yield: 24%; (e) EDC·HCl, 4-DMAP, CHCl₃, 50 °C, 16 h; (f) trifluoroacetic acid, methylene chloride, yield: 49%; and (g) THF, mesyl chloride (**73**), pyridine, reflux, 16 h, yield: 14%.

derivative **95**, which was then esterified to 4-(3-acetoxyoxetan-3-yl)benzoic acid (**96**). An amide bond formation with **30** using EDC·HCl and 4-DMAP then yielded **97**, which was reacted with mesylchloride (**73**) in the presence of pyridine to obtain **98** before basic cleavage of the acetyl group afforded **25** (Scheme 8).

Scheme 8. Synthesis of 25^a

^aReagents and conditions: (a) *n*-BuLi, 3-oxetanone (**94**), THF, −78 °C, 1.5 h, yield: 48%; (b) acetyl chloride, DCM, NEt₃, reflux, 16 h, yield: 70%; (c) EDC·HCl, 4-DMAP, CHCl₃, 50 °C, 16 h, yield: 49%; (d) mesyl chloride (**73**), THF, pyridine, reflux, 16 h, yield: 55%; and (e) LiOH, H₂O, EtOH, THF, 5 h, yield: 48%.

Biological Evaluation. FXR modulation by **4–29** was determined in a cellular reporter gene assay in transiently transfected HeLa cells using the heterodimer of the full-length human FXR and retinoid X receptor α (RXR α) to control the reporter gene expression. Both receptors were constitutively overexpressed (CMV promoter). Firefly luciferase under the control of the human FXR response element from the promoter region of the bile salt export protein (BSEP) served as reporter gene,³⁰ and constitutively expressed (SV40 promoter) renilla luciferase was used to normalize for transfection efficiency and test compound toxicity. Recombinant sEH protein and the fluorogenic substrate (3-phenyloxiranyl)acetic acid cyano-(6-methoxynaphthalen-2-yl)-

Table 1. Biological Activity and Microsomal Stability of 3, Its Metabolite 3a, and Derivatives 4–10^a


ID	R ¹	R ²	R ³	EC ₅₀ (FXR) (max. rel. act.)	IC ₅₀ (sEH)	t _{1/2} (in vitro)	CL _{int} ^b
3	-SO ₂ -Me	-Cl	-H	0.020±0.004 μM (35±1%)	0.0041±0.0004 μM	65±4 min	21±2
3a	-H	-Cl	-H	0.046±0.011 μM (29±1%)	0.040±0.006 μM	n.d.	n.d.
4	-SO ₂ -Et	-Cl	-H	0.50±0.05 μM (23±1%)	0.0061±0.0005 μM	47±3 min	28±2
5	-SO ₂ -iPr	-Cl	-H	0.42±0.02 μM (11±1%)	0.0112±0.0003 μM	59±8 min	23±3
6	-SO ₂ -cyclopropyl	-Cl	-H	1.5±0.3 μM (22±1%)	0.0078±0.0005 μM	33±3 min	41±4
7	-SO ₂ -CF ₃	-Cl	-H	inactive (30 μM)	0.021±0.005 μM	78±5 min	17±1
8	-SO ₂ -Me	-F	-H	inactive (30 μM)	0.016±0.001 μM	29±2 min	47±3
9	-SO ₂ -Me	-F	-F	inactive (30 μM)	0.085±0.001 μM	145±11 min	9.3±0.7
10	-SO ₂ -Me	-Cl	-Cl	inactive (30 μM)	0.268±0.008 μM	82±6 min	16±2

^aData are the mean ± standard error of the mean (SEM), $n \geq 3$. Inactive: no statistically significant activity at the indicated concentration.

^bIntrinsic clearance (RLM) in $\text{mg} \cdot \mu\text{L}^{-1} \cdot \text{min}^{-1}$.

methyl ester (PHOME) were used to characterize sEH inhibitory potency of 3–29.^{31,32} To capture metabolic stability, we incubated compounds 3–29 with rat liver microsomes (RLMs) and quantified the remaining amount of non-metabolized compound after 15, 30 and 60 min. The in vitro half-life was then determined using a logarithmic-linear transformation of the remaining amount of non-metabolized compound versus time. Intrinsic clearance was calculated based on in vitro half-life and normalized for the protein concentration in the microsomal reaction mixtures.^{33,34}

Structural Optimization. As our first attempt to stabilize the dual modulator chemotype against metabolic decay, we focused on the sulfonamide motif of 3 (Table 1) that is hydrolyzed in the formation of metabolite 3a. During the development of the FXRa/sEHi 3,¹² the sulfonamide motif turned out highly favorable to achieve the desired poly-pharmacological profile in terms of balanced dual potency but also to obtain sufficient solubility. Even its inversion or replacement by an amide was poorly tolerated. Additionally, 3 has exhibited strong therapeutic effects in several rodent models^{27,28} suggesting the chemotype as favorable and prompting us to conserve its scaffold as far as possible. To prevent hydrolysis of the methylsulfonamide, we hence introduced sterically more demanding ethyl- (4), isopropyl- (5), and cyclopropyl- (6) sulfonamides.

However, while these modifications were well tolerated by sEH, potency on FXR dropped substantially and microsomal stability was not enhanced. Replacing the methylsulfonamide (3) by a trifluoromethylsulfonamide (7) under the assumption that electron-withdrawing fluorine might boost metabolic stability was not tolerated by FXR either. Aiming to stabilize the sulfonamide through reduced electron density in the neighboring benzene ring, we varied its substitution pattern with fluorine substituents.

When chlorine (3) was replaced by fluorine (8), the stability still decreased and the potency on FXR was lost. A second fluorine substituent (9) caused a strong increase in microsomal stability but failed to reinstate the activity on FXR. The 3,5-dichloroderivative 10 exhibited intermediate stability but was neither tolerated by FXR nor favored by sEH.

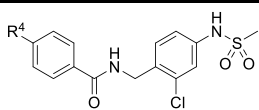
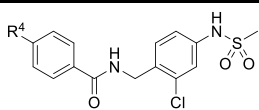
This initial SAR evaluation demonstrated that even small structural modifications in the alkylsulfonamide (4–7) or in the substitution pattern of the neighboring benzene moiety (8–10) resulted in a pronounced loss of activity on FXR. We therefore refrained from further SAR studies on the sulfonamide residue and focused our attention on the metabolically labile *tert*-butylbenzamide.

We commenced the structural optimization of *tert*-butylbenzamide toward improved metabolic stability by replacing the *tert*-butyl motif with known bioisosteres that have been validated as less labile in previous examples^{35,36} (Table 2). The trifluoromethylcyclopropyl analogue 11 indeed revealed markedly higher stability against microsomal degradation and was well tolerated by sEH but the potency on FXR dropped by a factor of 27. The bicyclo[1.1.1]pentane derivative 12 exhibited similarly diminished potency on FXR as 11, demonstrating that the *tert*-butyl motif is highly favored by this nuclear receptor. Additionally, 12 was less active on sEH than 3 and its microsomal stability represented only a weak improvement over the lead. Trifluoromethyl analogue 13 comprised the most preferable overall profile in this first series. It retained full inhibitory potency on sEH and revealed high microsomal stability. Potency of 13 on FXR only dropped slightly by a factor of 7 compared to 3. We also probed the replacement of the *tert*-butyl motif of 3 by a dimethylamine (14) or a methylether (15), which were both markedly less active on FXR than 3 while retaining high potency on sEH. Methoxy derivative 15 revealed preferably high microsomal stability.

We hypothesized that the pronounced loss in the activity observed for dimethylamine 14 and methylether 15 might result from their smaller substituent size prompting us to follow-up on these modifications with larger amine and ether residues (Table 2).

The SAR of cyclic amine substituents (16–19) indeed revealed a correlation between the substituent size and activity on FXR. Although the azetidine derivative 16 was a very weak FXR agonist, the pyrrolidine (17) and piperidine (18) analogues exhibited nanomolar potency on FXR. Regarding sEH inhibition, the differences in activity were less pronounced among amine derivatives 14 and 16–18 and covered an

Table 2. Biological Activity and Microsomal Stability of 11–29^a

ID					
		EC ₅₀ (FXR) (max. rel. act.)	IC ₅₀ (sEH)	t _{1/2} (in vitro)	CL _{int} ^b
3		0.020±0.004 μM (35±1%)	0.0041±0.0004 μM	65±4 min	21±2
11		0.54±0.02 μM (31±1%)	0.0043±0.0004 μM	182±28 min	7.5±1.2
12		0.56±0.09 μM (19±1%)	0.049±0.002 μM	81±7 min	17±2
13		0.14±0.02 μM (20±1%)	0.007±0.001 μM	146±34 min	9.6±2.2
14		1.46±0.02 μM (17±1%)	0.045±0.002 μM	53±4 min	25±2
15		inactive (30 μM)	0.038±0.005 μM	270±23 min	5.0±0.5
16		13±7 μM (21±1%)	0.094±0.005 μM	157±13 min	8.6±0.7
17		0.25±0.01 μM (27±1%)	0.041±0.004 μM	77±4 min	17±1
18		0.41±0.08 μM (28±1%)	0.071±0.005 μM	67±4 min	20±2
19		4.4±0.7 μM (18±1%)	0.175±0.008 μM	343±76 min	4.1±0.9
20		1.09±0.02 μM (12±1%)	0.022±0.001 μM	148±10 min	9.1±0.7
21		2.2±0.07 μM (17±1%)	0.031±0.002 μM	108±5 min	12±1
22		0.4±0.1 μM (19±1%)	0.012±0.001 μM	111±16 min	12±2
23		0.032±0.003 μM (20±1%)	0.17±0.01 μM	1210±603 min	1.5±0.8
24		inactive (30 μM)	0.009±0.001 μM	55±5 min	24±3
25		inactive (30 μM)	0.111±0.004 μM	254±47 min	5.4±1.1
26		1.2±0.1 μM (19±1%)	0.002±0.001 μM	141±13 min	9.6±0.9
27		4.0±0.5 μM (19±1%)	0.013±0.001 μM	62±5 min	22±2
28		3.22±0.05 μM (21±1%)	0.004±0.001 μM	96±11 min	14±2
29		inactive (30 μM)	0.010±0.001 μM	138±15 min	9.8±1.1
30		unstable			

^aLead compound 3 for comparison. Data are the mean ± SEM, $n \geq 3$. Inactive: no statistically significant activity at the indicated concentration.

^bIntrinsic clearance (RLM) in $\text{mg} \cdot \mu\text{L}^{-1} \cdot \text{min}^{-1}$.

intermediate nanomolar range. The more polar morpholino derivative 19 was not favored by FXR and sEH. The microsomal stability and on-target activity of 14 and 16–19 revealed opposing trends, wherein the least active compounds 16 and 19 comprised the highest stability.

Following up on methyl ether derivative 15, which possessed very high microsomal stability, we first combined the ether moiety with the favored trifluoromethyl substituent of 13 in trifluoromethoxy analogue 20, which retained high stability and was a potent sEH inhibitor, but the FXR agonism decreased markedly compared to 3. We then extended the size

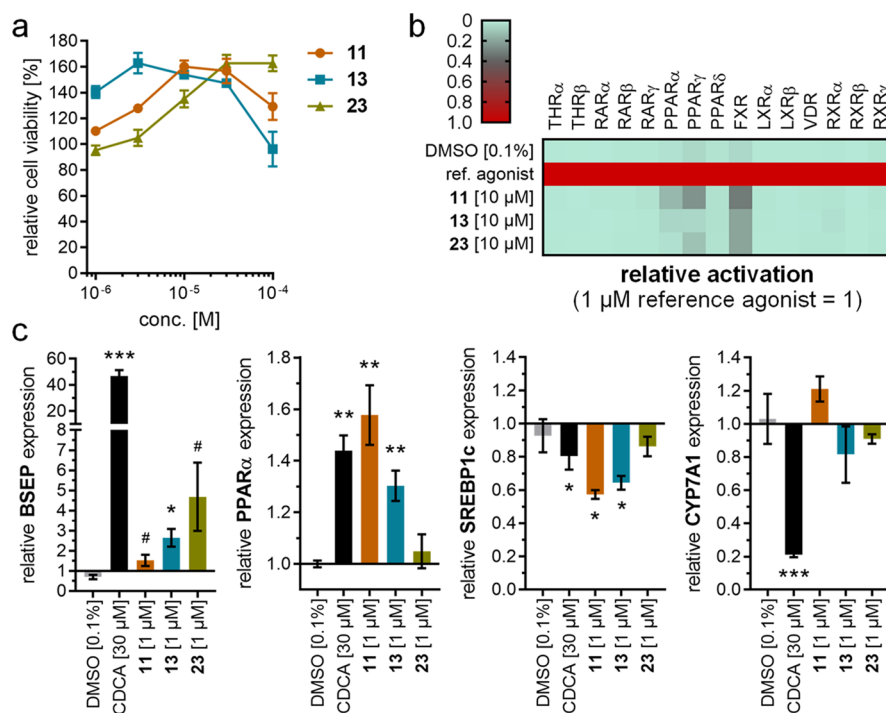


Figure 1. In vitro profiling of dual FXR/sEH modulators **11**, **13**, and **23**. (a) **11**, **13**, and **23** were nontoxic up to 100 μM in HepG2 cells in a WST-1 assay. Data are the mean \pm SEM; $n = 3$. (b) **11**, **13**, and **23** were selective over related nuclear receptors except for weak PPAR α and PPAR γ activation by **11** at 10 μM . Heatmap shows mean relative nuclear receptor activation vs reference agonists (1 μM); $n \geq 2$. (c) **11**, **13**, and **23** (at 1 μM) modulated FXR-regulated gene expression in HepG2 cells with induction of BSEP and PPAR α , and downregulation of SREBP1c. CYP7A1 expression was not affected. Data are mean \pm SEM relative mRNA expression determined by the $2^{-\Delta\Delta\text{Ct}}$ method with GAPDH as a reference gene; $n = 4$. # $p < 0.1$, * $p < 0.05$, ** $p < 0.01$, *** $p < 0.001$ (t -test vs DMSO-treated cells).

of the ether substituent from methyl (**15**) over ethyl (**21**) to isopropyl (**22**) and observed increasing FXR agonism with larger substituent size while sEH inhibitory potency was less affected but slightly increased, too. Microsomal stability, despite dropping with replacement of methyl by larger alkyl residues, remained superior compared to **3**. Oxygen-containing *tert*-butyl mimicking motifs, therefore, appeared to be promising. We hypothesized that increasing polarity in this region could further enhance microsomal stability and inverted the ether motif to the tertiary alcohol **23**, which indeed was exceptionally stable against degradation by liver microsomes. Moreover, **23** emerged as the first stabilized analogue of **3** with double-digit nanomolar potency on FXR. The 2-hydroxypropyl substituent of **23** was less favored by sEH but still exhibited submicromolar inhibitory potency. When the hydroxyl group was methylated in **24**, the activity on sEH was strongly enhanced but the microsomal stability dropped dramatically. Additionally, **24** as well as hydroxyoxetane **25** failed to activate FXR, which again highlighted the challenge of replacing the *tert*-butyl motif without loss of activity on FXR. Despite its weaker sEH inhibitory potency, **23** therefore emerged as another substantial improvement over **3**. Overall, fluorinated *tert*-butyl mimetics such as **11** and **13** had shown favorable profiles prompting us to study further fluorine-containing alkyl substituents in this region (Table 2). 1,1-Difluoroethyl (**26**) and 2,2,2-trifluoroethyl (**27**) as well as the merged pentafluoroethyl (**28**) analogues exhibited strong sEH inhibition, while FXR agonism compared to the trifluoromethylcyclopropyl derivative **11** and the smaller trifluoromethyl analogue **13** was decreased. Interestingly, microsomal stability varied markedly among the fluorinated derivatives. Although the trifluoromethyl derivative **13** was very stable, pentafluor-

oethyl (**28**) and especially 2,2,2-trifluoroethyl (**27**) substituents resulted in significantly lower stability. The 1,1-difluoroethyl (**26**) as well as the trifluoromethylcyclopropyl (**11**) derivatives comprised intermediate but sufficient stability.

The pentafluorosulfanyl moiety has been proposed as another suitable bioisosteric replacement of *tert*-butyl and trifluoromethyl groups.³⁷ We incorporated this motif in the dual modulator chemotype (**29**) and indeed observed improved microsomal stability compared to the *tert*-butyl lead compound **3**; **29** also retained high potency on sEH but was inactive on FXR.

In our endeavor to design second-generation dual modulators of FXR and sEH with improved metabolic stability, we discovered three structural modifications (**11**, **13**, **23**) that retained sufficient potency on the protein targets and simultaneously generated a substantial improvement in microsomal stability. Achieving high potency on FXR emerged as the greatest challenge in this multi-objective optimization. In an attempt to combine the most favorable modifications and to obtain further optimization, we designed the fused compound **30** representing a combination of **11** and **23**; **30** was synthesized but the 1-hydroxycyclopropyl substituent turned out unstable and underwent a rearrangement to an ethylmethyl ketone.³⁸ Hence, **11**, **13**, and **23** evolved as the most favorable second-generation dual FXR activators/sEH inhibitors for further in vitro and in vivo profiling.

In Vitro and In Vivo Profiling. All three dual modulators **11**, **13**, and **23** exhibited no toxic effects in HepG2 cells up to 100 μM concentration as determined in a WST-1 assay (Figure 1a) and were highly selective over related nuclear receptors at 10 μM apart from weak PPAR α and PPAR γ activation by **11**

(Figure 1b). Aqueous solubility was sufficient for **11** (2.9 mg/L) and **13** (5.7 mg/L) and high for **23** (48 mg/L).

To confirm FXR target engagement in a native and orthogonal cellular setting, we treated FXR-expressing human hepatocytes (HepG2) with **11**, **13**, or **23** (each at 1 μ M) and studied the effects on FXR-regulated gene expression by quantitative real-time polymerase chain reaction (qRT-PCR). The endogenous FXR agonist chenodeoxycholic acid (CDCA) served as the positive control. In line with their partial agonism in the BSEP-based reporter gene assay, **13** and **23** induced BSEP mRNA expression with low efficacy compared to CDCA, whereas **11** exhibited very weak BSEP induction (Figure 1c). **11** and **13** efficiently promoted the expression of peroxisome proliferator-activated receptor α (PPAR α) and downregulated sterol regulatory element-binding protein 1c (SREBP1c), while **23** had no observable effect on both FXR-regulated genes. Similar to our observations of weak effects of the lead compound **3**^{12,28} and other partial agonists^{39–41} on cholesterol-7 α -hydroxylase (CYP7A1) expression, **11**, **13**, and **23** did not suppress CYP7A1.

The second-generation FXRa/sEHi **13** consistently exhibited potent partial FXR agonism in the reporter gene assay and in hepatocytes and potently inhibited sEH. Additionally, **13** revealed the most favorable selectivity profile among nuclear receptors and comprised the desired high stability against microsomal degradation. With these characteristics, **13** met all criteria of our objective to develop a potent FXRa/sEHi resembling the biological activity profile of **3** with improved metabolic stability. Hence, we determined the PK profile of **13** in mice, which remarkably confirmed the envisioned improved pharmacokinetics (Figure 2). A single

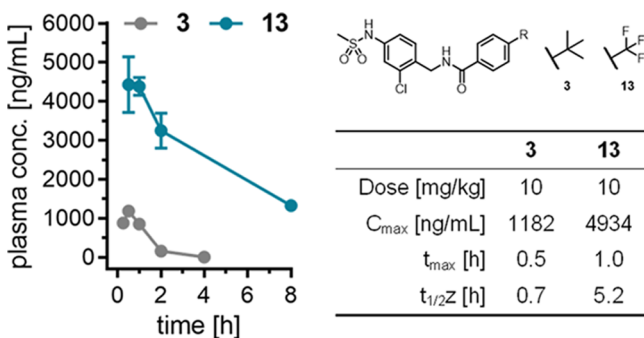


Figure 2. Pharmacokinetic profile and parameters of **13** in mice after a single oral dose of 10 mg/kg. Lead compound **3** for comparison. The pharmacokinetic profile of **3** in mice has been determined previously¹² under equal conditions as for **13** (vehicle, dose, administration route).

oral 10 mg/kg dose of **13** resulted in a maximum plasma level of 4.9 μ g/mL and a half-life of 5.2 h, presenting as a pronounced improvement in exposure over the lead compound **3** (c_{max} 1.2 μ g/mL, t_{1/2} 0.7 h).

CONCLUSIONS

Following the hypothesis that the treatment of the multifactorial pathology NAFLD/NASH would benefit from combined multiple modes of action, we have previously developed a potent dual FXR/sEH modulator chemotype.¹² In vivo characterization of the original dual FXR activator/sEH inhibitor **3** has demonstrated remarkable therapeutic efficacy in toxin- and diet-induced rodent models of NASH as a

preventive²⁷ and curative²⁸ intervention. These results from animal studies have confirmed our polypharmacology hypothesis and characterized dual FXR/sEH modulation as an attractive strategy to treat NASH. However, while being highly potent on the intended targets, the original dual modulator **3** is characterized by a short half-life and moderate plasma levels in vivo leading to the need of twice-daily dosing. Aiming to overcome this pharmacokinetic liability, we have further studied the structure–activity and structure–stability relationships of the dual modulator chemotype in a multi-objective optimization endeavor. Based on the known metabolic degradation pathways of **3**, we have first probed stabilization of the sulfonamidophenyl motif, but modifications in this region were poorly tolerated by FXR and failed to provide substantial metabolic stabilization. Structural variations of the labile *tert*-butyl motif were more suitable to stabilize the scaffold against microsomal degradation but retaining high potency on FXR presented as a challenge, which agrees with the privileged role of the *tert*-butylphenyl motif in partial FXR agonists.^{39–43} In vitro, replacement of *tert*-butyl motif by trifluoromethylcyclopropyl (**11**), trifluoromethyl (**13**), and hydroxyisopropyl (**23**) residues emerged as most favorable modifications to retain dual potency and achieve metabolic stabilization. Based on its potency, preferable selectivity, and robust effects on FXR-regulated gene expression in hepatocytes, we chose the second-generation dual modulator **13** for in vivo pharmacokinetic profiling, the results of which confirmed the intended improvement over the original compound **3**. With peak plasma levels of 4.9 μ g/mL and a half-life above 5 h, **13** overcomes the pharmacokinetic liabilities of **3** and retains the attractive polypharmacological activity profile of the lead. These characteristics render **13** suitable for late-stage preclinical development to move the therapeutic concept of dual FXR/sEH modulation toward clinical trials.

EXPERIMENTAL SECTION

Chemistry. General. All chemicals and solvents were of reagent grade and were used without further purification unless otherwise specified. All reactions were conducted in oven-dried glassware under argon atmosphere and in absolute solvents. NMR spectra were recorded on a Bruker AV 500, Bruker AV 400, Bruker AV 300, or a Bruker am250xp spectrometer (Bruker Corporation, Billerica, MA). Chemical shifts (δ) are reported in ppm relative to tetramethylsilane (TMS) as reference. Multiplicity is reported: s, singlet; d, doublet; dd, doublet of doublets; t, triplet; and m, multiplet. Approximate coupling constants (*J*) are given in hertz (Hz). Mass spectra were obtained on a VG Platform II (Thermo Fischer Scientific, Inc., Waltham, MA) using electrospray ionization (ESI). High-resolution mass spectra were recorded on a MALDI LTQ ORBITRAP XL instrument (Thermo Fisher Scientific). Preparative HPLC was performed on a Shimadzu preparative LC-20A Prominence (Shimadzu, Kyoto, Japan) under the following conditions: column, Luna (10 μ m C18(2)) 100 \AA ; 250 \times 21.2 mm²; Phenomenex, Torrance, CA); mobile phase, isocratic 50:50 acetonitrile/H₂O + 0.1 formic acid for 30 min at a flow rate of 21 mL/min, and UV detection at 245 and 280 nm. Compound purity was analyzed on a Waters 600 Controller HPLC (Waters, Milford, MA) using a Waters 2487 dual absorbance detector and a Waters 717 plus Autosampler or a VWR Chromaster (VWR, Radnor, PA) with a 5160 pump system, using a DAD 5430 and a 5260 Autosampler both equipped with a MultoHigh100 RP18-5 μ m 250 \times 4 mm² column (CS-Chromatographie Service GmbH, Langerwehe, Germany) using a gradient (H₂O + 0.1% formic acid/MeOH 80:20 isocratic for 5 min to MeOH after additional 45 min and MeOH for additional 10 min) at a flow rate of 1 mL/min or a gradient (H₂O + 0.1% formic acid/MeOH 60:40 isocratic for 5 min to MeOH after additional 25 min

and MeOH for additional 10 min) at a flow rate of 1 mL/min with UV detection at 245 and 280 nm. All compounds used for biological characterization had a purity $\geq 95\%$. Precursors **30** and **52** and compound **3** have been reported previously.¹²

4-(1-(Trifluoromethyl)cyclopropyl)-N-(2-chloro-4-(methylsulfonamido)benzyl)benzamide (11). *N*-(4-Amino-2-chlorobenzyl)-4-(1-(trifluoromethyl)cyclopropyl)benzamide (**55**, 0.104 g, 0.282 mmol, 1.00 equiv) was dissolved in a mixture of THF (28 mL) and pyridine (2.8 mL). Methanesulfonyl chloride (**73**, 0.323 g, 2.82 mmol, 10.0 equiv) was added dropwise. The reaction mixture was stirred at reflux for 16 h. Then, aqueous hydrochloric acid (10%, 30 mL) was added and the phases were separated. The aqueous layer was extracted with EtOAc (3 \times 30 mL). The combined organic layers were dried over Na₂SO₄ and the solvent was removed in vacuum. The crude product was purified by column chromatography using *n*-hexane/EtOAc (1:1) as the mobile phase to obtain **11** as a colorless solid (0.052 g, 41%). ¹H NMR (500 MHz, DMSO-*d*₆) δ = 9.93 (s, 1H), 9.04 (s, 1H), 7.91 (d, *J* = 8.3 Hz, 2H), 7.57 (d, *J* = 8.1 Hz, 2H), 7.32 (d, *J* = 8.4 Hz, 1H), 7.26 (d, *J* = 2.1 Hz, 1H), 7.15 (dd, *J* = 8.4, 2.1 Hz, 1H), 4.48 (d, *J* = 5.7 Hz, 2H), 3.02 (s, 3H), 1.38 (s, 2H), 1.17 (s, 2H). ¹³C NMR (126 MHz, MeOD) δ = 169.74, 141.13, 139.98, 135.45, 134.93, 132.85, 132.52, 131.10, 128.53, [130.97, 128.80, 126.64, 124.47], 121.72, 119.59, 42.16, 39.37, [29.48, 29.21, 28.95, 28.68], [10.45, 10.44, 10.43, 10.42]. HRMS (MALDI): *m/z* calcd 469.05710 for C₁₉H₁₈ClF₃N₂O₃Na, found 469.05613 [M + Na]⁺.

4-(Trifluoromethyl)-N-(2-chloro-4-(methylsulfonamido)benzyl)benzamide (13). *N*-(4-Amino-2-chlorobenzyl)-4-(trifluoromethyl)benzamide (**57**, 0.126 g, 0.383 mmol, 1.00 equiv) was dissolved in a mixture of THF (25 mL) and pyridine (2.5 mL). Methanesulfonyl chloride (**73**, 0.439 g, 3.83 mmol, 10.0 equiv) was added dropwise. The reaction mixture was stirred at reflux for 16 h. Then, aqueous hydrochloric acid (10%, 25 mL) was added and the phases were separated. The aqueous layer was extracted with EtOAc (3 \times 25 mL). The combined organic layers were dried over Na₂SO₄ and the solvent was removed in vacuum. The crude product was purified by column chromatography using *n*-hexane/EtOAc (1:1) as the mobile phase to obtain **13** as a colorless solid (0.042 g, 27%). ¹H NMR (500 MHz, acetone-*d*₆) δ = 8.71 (s, 1H), 8.40 (t, *J* = 5.9 Hz, 1H), 8.07–8.00 (m, 2H), 7.75–7.66 (m, 2H), 7.36 (d, *J* = 8.4 Hz, 1H), 7.31 (d, *J* = 2.3 Hz, 1H), 7.15 (dd, *J* = 8.4, 2.3 Hz, 1H), 4.57 (d, *J* = 5.8 Hz, 2H), 2.93 (s, 3H). ¹³C NMR (126 MHz, acetone-*d*₆) δ = 166.50, 139.65, [139.12, 139.11, 139.10, 139.09], 134.21, [133.47, 133.22, 132.96, 132.70], 132.63, 131.13, 128.98, [128.21, 126.05, 123.88, 121.72], [126.27, 126.24, 126.21, 126.18], 121.16, 119.34, 41.68, 39.68. HRMS (MALDI): *m/z* calcd 407.04385 for C₁₉H₁₉ClF₃N₂O₃S, found 407.04364 [M + H]⁺.

4-(2-Hydroxypropan-2-yl)-N-(2-chloro-4-(methylsulfonamido)benzyl)benzamide (23). *N*-(4-Amino-2-chlorobenzyl)-4-(2-hydroxypropan-2-yl)benzamide (**67**, 0.103 g, 0.323 mmol, 1.00 equiv) was dissolved in a mixture of THF (5 mL) and pyridine (5 mL) and cooled to 0 °C. Methanesulfonyl chloride (**73**, 0.111 g, 0.969 mmol, 3.00 equiv) was added dropwise at 0 °C. The reaction mixture was stirred at 0 °C for 8 h. Then, aqueous hydrochloric acid (10%, 25 mL) was added and the phases were separated. The aqueous layer was extracted with ethyl acetate (3 \times 30 mL). The combined organic layers were dried over Na₂SO₄ and the solvents were removed in vacuum. Further purification was performed by column chromatography using *n*-hexane/EtOAc (5:3) as the mobile phase to obtain **23** as a colorless solid (6 mg, 5%). ¹H NMR (500 MHz, methanol-*d*₄) δ = 7.85–7.82 (m, 2H), 7.59 (d, *J* = 8.4 Hz, 2H), 7.37–7.33 (m, 2H), 7.16 (dd, *J* = 8.4, 2.3 Hz, 1H), 4.62 (s, 2H), 2.96 (s, 3H), 1.54 (s, 6H). ¹³C NMR (126 MHz, methanol-*d*₄) δ = 168.80, 153.67, 138.51, 133.49, 129.62, 127.96, 126.87, 126.60, 124.48, 120.35, 118.23, 71.51, 40.70, 37.98, 30.39. HRMS (MALDI): *m/z* calcd 419.08028 for C₁₈H₂₁ClN₂O₄Na, found 419.08020 [M + Na]⁺.

4-(1-(Trifluoromethyl)cyclopropan-1-yl)benzoic Acid (45). Pd(OAc)₂ (0.010 g, 0.045 mmol, 0.03 equiv) and Xantphos (0.010 g, 0.045 mmol, 0.03 equiv) were dissolved in DMF (10 mL). Formic acid (0.400 mL, 10.7 mmol, 7.00 equiv) and 1-bromo-4-(1-(trifluoromethyl)cycloprop-1-yl)benzene (**81**, 1.51 mmol, 0.400 g,

1.00 equiv) were added dropwise. Then, EDC-HCl (0.058 g, 0.301 mmol, 0.200 equiv) and triethylamine (0.305 g, 3.02 mmol, 2.00 equiv) were added and the mixture was stirred at 50 °C for 20 h. After cooling to room temperature, aqueous hydrochloric acid (10%, 10 mL) was added and the mixture was extracted with EtOAc (3 \times 30 mL). The combined organic layers were extracted with a saturated aqueous solution of Na₂CO₃ (3 \times 30 mL). Then, the combined aqueous layers were brought to pH 1 with concentrated aqueous hydrochloric acid and extracted with EtOAc (3 \times 30 mL). The combined organic layers were dried over Na₂SO₄ and the solvent was evaporated in vacuum to obtain **45** as a beige solid (0.177 g, 51%). ¹H NMR (300 MHz, DMSO-*d*₆) δ = 12.89 (s, 1H), 7.98–7.90 (m, 2H), 7.62–7.54 (m, 2H), 1.44–1.33 (m, 2H), 1.22–1.14 (m, 2H). ¹³C NMR (75 MHz, DMSO-*d*₆) δ = 166.87, 140.02, 131.18, 130.86, 129.41, [131.78, 128.15, 124.52, 121.15], [28.16, 27.75, 27.32, 26.88], [9.81, 9.77, 9.74, 9.71].

4-(2-Hydroxypropan-2-yl)benzoic Acid (49). 4-Isopropylbenzoic acid (**85**, 0.700 g, 4.26 mmol, 1.00 equiv) was dissolved in a mixture of H₂O (15 mL) and pyridine (15 mL). After stirring at 100 °C for 1 h, KMnO₄ (2.02 g, 12.8 mmol, 3.00 equiv) was added and the resulting reaction mixture was stirred at 100 °C for 16 h. After cooling to room temperature, aqueous sodium hydroxide solution (10%, 50 mL) was added and the mixture was filtered. The filtrate was brought to pH 1 using concentrated aqueous hydrochloric acid and extracted with EtOAc (3 \times 30 mL). The combined organic layers were dried over Na₂SO₄ and the solvent was evaporated in vacuum. Further purification was performed by column chromatography using hexane/acetone (9:2) as the mobile phase to obtain **49** as a colorless solid (0.352 g, 46%). ¹H NMR (400 MHz, DMSO-*d*₆) δ = 7.87 (d, *J* = 8.2 Hz, 2H), 7.57 (d, *J* = 8.2 Hz, 2H), 5.16 (s, 1H), 1.43 (s, 5H). ¹³C NMR (101 MHz, DMSO-*d*₆) δ = 167.31, 155.50, 128.92, 128.57, 124.69, 70.74, 31.66.

N-(4-Amino-2-chlorobenzyl)-4-(1-(trifluoromethyl)cyclopropyl)benzamide (55). 4-(1-(Trifluoromethyl)cyclopropyl)benzoic acid (**45**, 0.153 g, 0.665 mmol, 1.00 equiv), 1-(4-amino-1-chlorophenyl)methanamine (**30**, 0.312 g, 1.99 mmol, 3.00 equiv), and 4-DMAP (0.081 g, 0.665 mmol, 1.00 equiv) were dissolved in a mixture of CHCl₃ (25 mL) and DMF (2.5 mL). After cooling the reaction mixture to 0 °C, EDC-HCl (0.382 g, 1.99 mmol, 3.00 equiv) was added and the mixture was stirred at 0 °C for 30 min and at 50 °C for 16 h. Then, aqueous hydrochloric acid (10%, 30 mL) was added and the phases were separated. The aqueous layer was brought to pH 12 using Na₂CO₃ and extracted with EtOAc (3 \times 30 mL). The combined organic layers were dried over Na₂SO₄ and the solvent was removed in vacuum. The crude product was purified by column chromatography using *n*-hexane/EtOAc (4:3) as the mobile phase to obtain **55** as a yellow solid (0.125 g, 51%). ¹H NMR (300 MHz, acetone-*d*₆) δ = 7.95–7.90 (m, 2H), 7.57 (d, *J* = 8.1 Hz, 2H), 7.15 (d, *J* = 8.3 Hz, 1H), 6.72 (d, *J* = 2.3 Hz, 1H), 6.58 (dd, *J* = 8.3, 2.3 Hz, 1H), 4.85 (s, 1H), 4.54 (d, *J* = 5.6 Hz, 2H), 1.39 (dd, *J* = 6.9, 5.0 Hz, 2H), 1.18–1.12 (m, 2H). ¹³C NMR (75 MHz, DMSO-*d*₆) δ = 166.17, 149.60, [138.79, 138.78], [135.95, 132.33, 128.71, 125.08], 134.96, 132.91, 131.39, 130.23, 127.94, 122.79, 114.07, 113.09, 40.60, [28.58, 28.14, 27.70, 27.26], [10.21, 10.18, 10.15, 10.12].

N-(4-Amino-2-chlorobenzyl)-4-(trifluoromethyl)benzamide (57). 4-(Trifluoromethyl)benzoic acid (**35**, 0.200 g, 0.912 mmol, 1.00 equiv), 1-(4-amino-1-chlorophenyl)methanamine (**30**, 0.429 g, 2.74 mmol, 3.00 equiv), and 4-DMAP (0.111 g, 0.912 mmol, 1.00 equiv) were dissolved in a mixture of CHCl₃ (30 mL) and DMF (3 mL). After cooling the reaction mixture to 0 °C, EDC-HCl (0.525 g, 2.74 mmol, 3.00 equiv) was added and the mixture was stirred at 0 °C for 30 min and at 50 °C for 16 h. Then, aqueous hydrochloric acid (10%, 30 mL) was added and the phases were separated. The aqueous layer was brought to pH 12 using Na₂CO₃ and extracted with EtOAc (3 \times 30 mL). The combined organic layers were dried over Na₂SO₄ and the solvent was removed in vacuum. The crude product was purified by column chromatography using *n*-hexane/EtOAc (4:3) as the mobile phase to obtain **57** as a yellow solid (0.126 g, 42%). ¹H NMR (300 MHz, DMSO-*d*₆) δ = 9.02 (t, *J* = 5.2 Hz, 1H), 8.07 (d, *J* = 8.2 Hz, 2H), 7.84 (d, *J* = 8.2 Hz, 2H), 7.04 (d, *J* = 8.3 Hz, 1H), 6.63 (d, *J*

= 2.2 Hz, 1H), 6.49 (dd, $J = 8.3, 2.1$ Hz, 1H), 5.30 (s, 2H), 4.40 (d, $J = 5.5$ Hz, 2H). ^{13}C NMR (75 MHz, acetone- d_6) $\delta = 166.13, 150.09, 139.50, 134.43, [133.56, 133.13, 132.70, 132.28], 131.67, [130.44, 126.84, 123.23, 119.63], 128.95, [126.21, 126.16, 126.11, 126.06], 124.07, 115.21, 113.88, 41.81$.

***N*-(4-Amino-2-chlorobenzyl)-4-(2-hydroxypropan-2-yl)-benzamide (67).** 4-(2-Hydroxypropan-2-yl)benzoic acid (49, 0.103 g, 0.572 mmol, 1.00 equiv), 1-(4-amino-1-chlorophenyl)methanamine (30, 0.134 g, 0.857 mmol, 1.50 equiv), and 4-DMAP (0.007 g, 0.057 mmol, 0.10 equiv) were dissolved in a mixture of CHCl_3 (25 mL) and DMF (2.5 mL). After cooling the reaction mixture to 0 °C, EDC·HCl (0.131 g, 0.656 mmol, 1.20 equiv) was added and the mixture was stirred at 0 °C for 30 min and at 50 °C for 16 h. Then, aqueous hydrochloric acid (10%, 30 mL) was added and the phases were separated. The aqueous layer was brought to pH 12 using Na_2CO_3 and extracted with EtOAc (3 × 30 mL). The combined organic layers were dried over Na_2SO_4 and the solvent was removed in vacuum. The crude product was purified by column chromatography using *n*-hexane/EtOAc (3:5) as the mobile phase to obtain 67 as a yellow oil (0.104 g, 57%). ^1H NMR (400 MHz, methanol- d_4) $\delta = 7.83\text{--}7.77$ (m, 2H), 7.59–7.53 (m, 2H), 7.11 (d, $J = 8.2$ Hz, 1H), 6.75–6.74 (m, 1H), 6.60–6.57 (m, 1H), 4.53 (s, 2H), 1.54 (s, 6H). ^{13}C NMR (101 MHz, methanol- d_4) $\delta = 170.04, 154.79, 149.84, 134.87, 133.60, 131.30, 129.32, 128.21, 125.77, 116.45, 114.78, 72.87, 42.19, 31.76$.

Biological Characterization. BSEP-Based Full-Length FXR Reporter Gene Assay. Plasmids: pcDNA3-hFXR⁴⁴ contains the sequence of human FXR. pSG5-hRXR⁴⁵ contains the sequence of human RXR α . pGL3basic (Promega Corporation, Fitchburg, WI) with a shortened construct of the promoter of the bile salt export protein (BSEP) cloned into the *SacI/NheI* cleavage site in front of the luciferase gene was used as the reporter plasmid.⁴⁴ pRL-SV40 (Promega) served as a control for normalization of transfection efficiency and cell growth. Assay procedure: HeLa cells (German Collection of Microorganisms and Cell Culture GmbH, DSMZ) were grown in Dulbecco's modified Eagle's medium (DMEM) high glucose, supplemented with 10% fetal calf serum (FCS), sodium pyruvate (1 mM), penicillin (100 U/mL), and streptomycin (100 $\mu\text{g}/\text{mL}$) at 37 °C and 5% CO_2 ; 24 h before transfection, HeLa cells were seeded in 96-well plates with a density of 8000 cells/well; 3.5 h before transfection, the medium was changed to DMEM high glucose, supplemented with sodium pyruvate (1 mM), penicillin (100 U/mL), streptomycin (100 $\mu\text{g}/\text{mL}$), and 0.5% charcoal-stripped FCS. Transient transfection of HeLa cells with BSEP-pGL3, pRL-SV40, and the expression plasmids pcDNA3-hFXR and pSG5-hRXR was carried out using calcium phosphate transfection method; 16 h after transfection, the medium was changed to DMEM high glucose, supplemented with sodium pyruvate (1 mM), penicillin (100 U/mL), streptomycin (100 $\mu\text{g}/\text{mL}$) and 0.5% charcoal-stripped FCS. 24 h after transfection, the medium was changed to DMEM without phenol red, supplemented with sodium pyruvate (1 mM), penicillin (100 U/mL), streptomycin (100 $\mu\text{g}/\text{mL}$), L-glutamine (2 mM), and 0.5% charcoal-stripped FCS, now additionally containing 0.1% DMSO and the respective test compound or 0.1% DMSO alone as untreated control. Each concentration was tested in triplicate, and each experiment was repeated independently at least three times. Following 24 h incubation with the test compounds, cells were assayed for luciferase activity using the Dual-Glo Luciferase Assay System (Promega) according to the manufacturer's protocol. Luminescence was measured with a Tecan Infinite M200 luminometer (Tecan Deutschland GmbH, Crailsheim, Germany) or a Tecan Spark 10 M luminometer (Tecan). Normalization of transfection efficiency and cell growth was done by division of firefly luciferase data by renilla luciferase data multiplied by 1000 resulting in relative light units (RLU). Fold activation was obtained by dividing the mean RLU of a test compound at a respective concentration by the mean RLU of untreated control. Relative activation was obtained by dividing the fold activation of the test compound at a respective concentration by the fold activation of FXR full agonist GW4064 at 3 μM . EC_{50} and standard deviation were calculated with the mean relative activation values of at least three independent experiments set

up in triplicate by SigmaPlot 12.5 (Systat Software GmbH, Erkrath, Germany) using a four-parameter logistic regression. The assay was validated with FXR agonists OCA ($\text{EC}_{50} = 0.16 \pm 0.02$ μM , $87 \pm 3\%$ rel. max. act.) and GW4064 ($\text{EC}_{50} = 0.51 \pm 0.16$ μM , 3 μM defined as 100%).

sEH Activity Assay. sEH inhibitory potency was determined in a fluorescence-based 96-well sEH activity assay using purified recombinant human enzyme.³¹ Nonfluorescent (3-phenyloxiranyl)-acetic acid cyano-(6-methoxynaphthalen-2-yl)-methyl ester^{32,46} (PHOME) was used as a substrate, which is hydrolyzed by sEH to fluorescent 6-methoxynaphthaldehyde. Purified recombinant human sEH (in BisTris buffer, pH 7, with 0.1 mg/mL BSA containing a final concentration of 3 nM sEH and 0.01% Triton-X 100) was preincubated with test compounds (in DMSO, final DMSO concentration: 1.6%) for 30 min at room temperature. Then, the substrate was added (final concentration 60 μM), and hydrolysis of the substrate was determined by measuring fluorescent product formation on a Tecan Infinite F200 Pro (Tecan, $\lambda_{\text{em}} = 330$ nm, $\lambda_{\text{ex}} = 465$ nm) for 30 min (one point per minute). A blank control (no protein and no compound) as well as a positive control (no compound) were executed. All experiments were conducted in triplicate and repeated in three independent experiments. For IC_{50} calculation, the dose–response curves of increasing compound concentrations were recorded. IC_{50} and standard deviation were calculated from at least three independent experiments set up in triplicate in GraphPad Prism 7 using a four-parameter logistic regression.

Hybrid Reporter Gene Assays. The plasmids pFA-CMV-NR-LBD^{47–51} for hTHR α , hTHR β , hPPAR α , hPPAR γ , hPPAR δ , hRAR α , hRAR β , hRAR γ , hLXR α , hLXR β , hRXR α , hRXR β , hRXR γ , and hVDR coding for the Gal4 DNA binding domain fused to the hinge region and LBD of the canonical isoform of the respective nuclear receptor, Gal4-responsive pFR-Luc (Stratagene, La Jolla, CA; reporter), and pRL-SV40 (Promega; internal control) were used for the hybrid reporter gene assays. HEK293T cells (DSMZ) were cultured in DMEM high glucose, supplemented with 10% FCS, sodium pyruvate (1 mM), penicillin (100 U/mL), and streptomycin (100 $\mu\text{g}/\text{mL}$) at 37 °C and 5% CO_2 and seeded in 96-well plates (3 × 10⁴ cells/well) 24 h prior to transfection. Before transfection, the medium was changed to Opti-MEM without supplements, and transient transfection with pFR-Luc, pRL-SV40, and one pFA-CMV-NR-LBD clone was carried out with the Lipofectamine LTX reagent (Invitrogen, Carlsbad, CA) according to the manufacturer's protocol. Five hours after transfection, the medium was changed to Opti-MEM supplemented with penicillin (100 U/mL) and streptomycin (100 $\mu\text{g}/\text{mL}$) additionally containing 0.1% DMSO and the respective test compound or 0.1% DMSO alone as the untreated control. Each concentration was tested in duplicate, and each experiment was repeated independently at least two times. Following overnight (14–16 h) incubation, cells were assayed for luciferase activity using the Dual-Glo Luciferase Assay System (Promega) according to the manufacturer's protocol. Luminescence was measured with a Tecan Spark M luminometer (Tecan). Normalization of transfection efficiency and cell growth was done by division of firefly luciferase data by renilla luciferase data and multiplying the value by 1000 resulting in relative light units (RLU). Fold activation was obtained by dividing the mean RLU of the test compound by the mean RLU of the untreated control. Relative activation refers to fold reporter activation of a test compound divided by the fold activation of the respective reference agonist (PPAR α : GW7647; PPAR γ : pioglitazone; PPAR δ : L165,041; LXR α/β : T0901317; RXR $\alpha/\beta/\gamma$: bexarotene; RAR $\alpha/\beta/\gamma$: tretinoin; VDR: calcitriol; 1 μM each and THR α/β : 3,3',5-triiodo-L-thyronine; 0.1 μM). All hybrid assays were validated with the respective reference agonists, which yielded EC_{50} values in agreement with the literature.

Microsomal Stability Assay. The solubilized test compound (5 μL , final concentration 10 μM) was preincubated at 37 °C in 432 μL of phosphate buffer (0.1 M, pH 7.4) together with 50 μL of NADPH regenerating system (30 mM glucose-6-phosphate, 4 U/mL glucose-6-phosphate dehydrogenase, 10 mM NADP, 30 mM MgCl_2). After 5

min, the reaction was started by the addition of 13 μL of microsome mix from the liver of Sprague-Dawley rats (Invitrogen; 20 mg protein/mL in 0.1 M phosphate buffer) in a shaking water bath at 37 $^{\circ}\text{C}$. The reaction was stopped by adding 500 μL of ice-cold methanol at 0, 15, 30, and 60 min. The samples were centrifuged at 5000g for 5 min at 4 $^{\circ}\text{C}$, and the test compound was quantified from the supernatants by HPLC: the composition of the mobile phase was adapted to the test compound in a range of MeOH 40–90% and water (0.1% formic acid) 10–60%; flow rate: 1 mL/min; stationary phase: Purospher STAR, RP18, 5 μm , 125 \times 4, precolumn: Purospher STAR, RP18, 5 μm , 4 \times 4; detection wavelength: 254 and 280 nm; injection volume: 50 μL . Control samples were performed to check the test compound's stability in the reaction mixture: first control was without NADPH, which is needed for the enzymatic activity of the microsomes, second control was with inactivated microsomes (incubated for 20 min at 90 $^{\circ}\text{C}$), and third control was without the test compound (to determine the baseline). The amounts of the test compound were quantified by an external calibration curve. Data are expressed as the mean \pm SEM remaining compound from three independent experiments. In vitro half-life was calculated by a logarithmic-linear transformation of the remaining amounts of non-metabolized test compound versus time in GraphPad Prism 7. Intrinsic clearance was calculated based on the in vitro half-life and normalized for the protein concentration used in the microsomal reaction mixtures as described previously.^{33,34}

Cell Viability Assay (WST-1). HepG2 cells were grown in DMEM high glucose, supplemented with sodium pyruvate (1 mM), penicillin (100 U/mL), streptomycin (100 $\mu\text{g}/\text{mL}$), and 10% FCS and seeded in 96-well plates (3×10^4 cells/well). After 24 h, the medium was changed to DMEM high glucose, supplemented with penicillin (100 U/mL), streptomycin (100 $\mu\text{g}/\text{mL}$), and 1% charcoal-stripped FCS and cells were incubated with the test compounds at varying concentrations in DMEM containing 0.1% DMSO, Revlotron as positive control, or DMEM containing 0.1% DMSO as negative control. Each sample was set up in duplicate, and each experiment was performed in three independent repeats. After 48 h, WST-1 reagent (Roche Diagnostics International AG, Rotkreuz, Schweiz) was added to each well according to manufacturer's instructions. After 45 min incubation, absorption (450 nm/ reference: 620 nm) was determined with a Tecan Infinite M200 (Tecan Deutschland GmbH) and data were analyzed according to the manufacturer's protocol.

Quantification of FXR Regulated Gene Expression by Quantitative Real-Time PCR. FXR target gene quantification was performed as described previously.^{30,39} In brief, HepG2 cells were grown in DMEM high glucose, supplemented with sodium pyruvate (1 mM), penicillin (100 U/mL), streptomycin (100 $\mu\text{g}/\text{mL}$), and 10% FCS and seeded in 6-well plates (1×10^6 cells/well). After 24 h, the medium was changed to MEM supplemented with L-glutamine (2 mM), penicillin (100 U/mL), streptomycin (100 $\mu\text{g}/\text{mL}$), and 1% charcoal-stripped FCS. After further 24 h, HepG2 cells were incubated with test compounds 11, 13, and 23 (1 μM) or CDCA (30 μM) in the same medium additionally containing 0.1% DMSO, or the medium with 0.1% DMSO alone as untreated control for 8 h, harvested, washed with cold phosphate-buffered saline (PBS) and then directly used for RNA extraction with the total RNA Mini Kit (R6834-02, Omega Bio-Tek, Inc., Norcross, GA). RNA (2 μg) was reverse-transcribed using the high-capacity cDNA reverse transcription kit (4368814, Thermo Fischer Scientific, Inc.) according to the manufacturer's protocol. FXR-regulated gene expression was then evaluated by quantitative real-time PCR analysis with a StepOnePlus System (Life Technologies, Carlsbad, CA) using PowerSYBRGreen (Life Technologies; 12.5 $\mu\text{L}/\text{well}$). Each sample was set up in duplicate and repeated in four independent experiments. Data were analyzed by the comparative $\Delta\Delta\text{Ct}$ method with glyceraldehyde 3-phosphate dehydrogenase (GAPDH) as the reference gene. The following PCR primers were used: GAPDH: 5'-ATA TGA TTC CAC CCA TGG CA-3' (fwd) and 5'-GAT GAT GAC CCT TTT GGC TC-3' (rev); CYP7A1: 5'-CAC CTT GAG GAC GGT TCC TA-3' (fwd) and 5'-CGA TCC AAA GGG CAT GTA GT-3' (rev); SREBP1c: 5'-GGA GGG GTA GGG CCA ACG GCC T-3' and 5'-CAT GTC

TTC GAA AGT GCA ATC C-3' (rev); PPAR α : 5'-GCT GTC ACC ACA GTA GCT TGG A-3' and 5'-GTG ATG ACC GAG CCA TCT GA-3' (rev); BSEP: 5'-CAT GGT GCA AGA AGT GCT GAG T-3' and 5'-AAG CGA TGA GCA ACT GAA ATG AT-3' (rev).

In Vivo PK Study. The PK study was performed by the contract research organization Pharmacelsus (Saarbrücken, Germany). All experimental procedures were approved by and conducted in accordance with the regulations of the local animal welfare authorities (Landesamt für Gesundheit und Verbraucherschutz, Abteilung Lebensmittel- und Veterinärwesen, Saarbrücken). Three male CD1 mice (32–34 g body weight, purchased from Janvier Labs, France) were used in the study. The animals were housed in a temperature-controlled room (20–24 $^{\circ}\text{C}$) and maintained in a 12 h light/12 h dark cycle. Food and water were available ad libitum. The animals received a single oral dose of 10 mg/kg body weight of the FXR α /sEHi 13 in water containing 1% HPMC/Tween 80 (99:1). The animals behaved normal throughout the study and showed no adverse effects. At four time points (30, 60, 120, and 480 min after application of 13), plasma samples (80 μL Li-heparin plasma) were obtained from the mice by puncture of the V. facialis. Compound 13 was quantified from the plasma samples by LC-MS. Pharmacokinetic analysis was performed with Kinetica 5.0 software (Thermo Scientific, Waltham).

■ ASSOCIATED CONTENT

Supporting Information

The Supporting Information is available free of charge at <https://pubs.acs.org/doi/10.1021/acs.jmedchem.1c00831>.

Synthetic procedures and analytical characterization data for compounds 4–29 and their precursors, as well as chromatographic purity analysis of 4–29 (PDF)

Molecular Formula strings contains structures of 4–29 and associated activity data (CSV)

■ AUTHOR INFORMATION

Corresponding Author

Daniel Merk – Institute of Pharmaceutical Chemistry, Goethe University Frankfurt, 60438 Frankfurt, Germany;
orcid.org/0000-0002-5359-8128; Phone: +49 69 79829327; Email: merk@pharmchem.uni-frankfurt.de

Authors

Moritz Helmstädter – Institute of Pharmaceutical Chemistry, Goethe University Frankfurt, 60438 Frankfurt, Germany
Astrid Kaiser – Institute of Pharmaceutical Chemistry, Goethe University Frankfurt, 60438 Frankfurt, Germany
Steffen Brunst – Institute of Pharmaceutical Chemistry, Goethe University Frankfurt, 60438 Frankfurt, Germany
Jurema Schmidt – Institute of Pharmaceutical Chemistry, Goethe University Frankfurt, 60438 Frankfurt, Germany
Riccardo Ronchetti – Institute of Pharmaceutical Chemistry, Goethe University Frankfurt, 60438 Frankfurt, Germany
Lilia Weizel – Institute of Pharmaceutical Chemistry, Goethe University Frankfurt, 60438 Frankfurt, Germany
Ewgenij Proschak – Institute of Pharmaceutical Chemistry, Goethe University Frankfurt, 60438 Frankfurt, Germany;
orcid.org/0000-0003-1961-1859

Complete contact information is available at: <https://pubs.acs.org/doi/10.1021/acs.jmedchem.1c00831>

Author Contributions

All authors have given approval to the final version of the manuscript.

Notes

The authors declare the following competing financial interest(s): The authors M.H., J.S., E.P. and D.M are inventors of the patents WO2018215610A1 and US62/902,771 which claim compounds reported in this manuscript and their uses. No other competing interests are declared.

ACKNOWLEDGMENTS

This research was financially supported by the Else-Kroener-Fresenius Foundation. D.M. is grateful for support by the Aventis Foundation. E.P. thanks Deutsche Forschungsgemeinschaft (DFG; Heisenberg-Professur PR1405/7-1) for financial support. R.R. received an “Erasmus Traineeship” from the University of Perugia.

ABBREVIATIONS USED

BSEP, bile salt export protein; CDCA, chenodeoxycholic acid; CYP7A1, cholesterol-7 α -hydroxylase; FXR, farnesoid X receptor; LXR, liver X receptor; NAFLD, non-alcoholic fatty liver disease; NASH, non-alcoholic steatohepatitis; OCA, obeticholic acid; RAR, retinoic acid receptor; PHOME, (3-phenyloxiranyl)acetic acid cyano-(6-methoxynaphthalen-2-yl)-methyl ester; PK, pharmacokinetic; PPAR, peroxisome proliferator-activated receptor; qRT-PCR, quantitative real-time polymerase chain reaction; RAR, retinoic acid receptor; RLM, rat liver microsomes; RXR, retinoid X receptor; sEH, soluble epoxide hydrolase; SREBP1c, sterol regulatory element-binding protein 1c; THR, thyroid hormone receptor; VDR, vitamin D receptor

REFERENCES

- (1) Vuppalanchi, R.; Noureddin, M.; Alkhoury, N.; Sanyal, A. J. Therapeutic Pipeline in Nonalcoholic Steatohepatitis. *Nat. Rev. Gastroenterol. Hepatol.* **2021**, *373*–392.
- (2) Buzzetti, E.; Pinzani, M.; Tsochatzis, E. A. The Multiple-Hit Pathogenesis of Non-Alcoholic Fatty Liver Disease (NAFLD). *Metabolism* **2016**, *65*, 1038–1048.
- (3) MacHado, M. V.; Diehl, A. M. Pathogenesis of Nonalcoholic Steatohepatitis. *Gastroenterology* **2016**, *150*, 1769–1777.
- (4) Diehl, A. M.; Day, C. Cause, Pathogenesis, and Treatment of Nonalcoholic Steatohepatitis. *N. Engl. J. Med.* **2017**, *377*, 2063–2072.
- (5) Tilg, H.; Adolph, T. E.; Moschen, A. R. Multiple Parallel Hits Hypothesis in Nonalcoholic Fatty Liver Disease: Revisited After a Decade. *Hepatology* **2021**, *73*, 833–842.
- (6) Pellicciari, R.; Fiorucci, S.; Camaioni, E.; Clerici, C.; Costantino, G.; Maloney, P. R.; Morelli, A.; Parks, D. J.; Willson, T. M. 6 α -Ethyl-Chenodeoxycholic Acid (6-ECDCA), a Potent and Selective FXR Agonist Endowed with Anticholestatic Activity. *J. Med. Chem.* **2002**, *45*, 3569–3572.
- (7) Mullard, A. FDA Rejects NASH Drug. *Nat. Rev. Drug Discovery* **2020**, *19*, 501.
- (8) Maloney, P. R.; Parks, D. J.; Haffner, C. D.; Fivush, A. M.; Chandra, G.; Plunket, K. D.; Creech, K. L.; Moore, L. B.; Wilson, J. G.; Lewis, M. C.; Jones, S.; Willson, T. M. Identification of a Chemical Tool for the Orphan Nuclear Receptor FXR. *J. Med. Chem.* **2000**, *43*, 2971–2974.
- (9) Neuschwander-Tetri, B. A.; Loomba, R.; Sanyal, A. J.; Lavine, J. E.; Van Natta, M. L.; Abdelmalek, M. F.; Chalasani, N.; Dasarthy, S.; Diehl, A. M.; Hameed, B.; Kowdley, K. V.; McCullough, A.; Terrault, N.; Clark, J. M.; Tonascia, J.; Brunt, E. M.; Kleiner, D. E.; Doo, E. Farnesoid X Nuclear Receptor Ligand Obeticholic Acid for Non-Cirrhotic, Non-Alcoholic Steatohepatitis (FLINT): A Multicentre, Randomised, Placebo-Controlled Trial. *Lancet* **2015**, *385*, 956–965.
- (10) Ratziu, V.; Harrison, S. A.; Franque, S.; Bedossa, P.; Leher, P.; Serfaty, L.; Romero-Gomez, M.; Boursier, J.; Abdelmalek, M.; Caldwell, S.; Drenth, J.; Anstee, Q. M.; Hum, D.; Hanf, R.; Roudot,

A.; Megnien, S.; Staels, B.; Sanyal, A.; et al. Elafibranor, an Agonist of the Peroxisome Proliferator-Activated Receptor- α and - δ , Induces Resolution of Nonalcoholic Steatohepatitis Without Fibrosis Worsening. *Gastroenterology* **2016**, *150*, 1147–1159e5.

(11) Proschak, E.; Stark, H.; Merk, D. Polypharmacology by Design: A Medicinal Chemist's Perspective on Multitargeting Compounds. *J. Med. Chem.* **2019**, *62*, 420–444.

(12) Schmidt, J.; Rotter, M.; Weiser, T.; Wittmann, S.; Weizel, L.; Kaiser, A.; Heering, J.; Goebel, T.; Angioni, C.; Wurglics, M.; Paulke, A.; Geisslinger, G.; Kahnt, A.; Steinhilber, D.; Proschak, E.; Merk, D. A Dual Modulator of Farnesoid X Receptor and Soluble Epoxide Hydrolase to Counter Nonalcoholic Steatohepatitis. *J. Med. Chem.* **2017**, *60*, 7703–7724.

(13) Gadaleta, R. M.; Cariello, M.; Sabbà, C.; Moschetta, A. Tissue-Specific Actions of FXR in Metabolism and Cancer. *Biochim. Biophys. Acta, Mol. Cell Biol. Lipids* **2015**, *1851*, 30–39.

(14) Pellicciari, R.; Costantino, G.; Fiorucci, S. Farnesoid X Receptor: From Structure to Potential Clinical Applications. *J. Med. Chem.* **2005**, *48*, 5383–5403.

(15) Jiang, C.; Xie, C.; Lv, Y.; Li, J.; Krausz, K. W.; Shi, J.; Brocker, C. N.; Desai, D.; Amin, S. G.; Bisson, W. H.; Liu, Y.; Gavrilova, O.; Patterson, A. D.; Gonzalez, F. J. Intestine-Selective Farnesoid X Receptor Inhibition Improves Obesity-Related Metabolic Dysfunction. *Nat. Commun.* **2015**, *6*, No. 10166.

(16) Mangels, N.; Awwad, K.; Wettenmann, A.; Dos Santos, L. R. B.; Frömel, T.; Fleming, I. The Soluble Epoxide Hydrolase Determines Cholesterol Homeostasis by Regulating AMPK and SREBP Activity. *Prostaglandins Other Lipid Mediators* **2016**, *125*, 30–39.

(17) Sun, C. C.; Zhang, C. Y.; Duan, J. X.; Guan, X. X.; Yang, H. H.; Jiang, H. L.; Hammock, B. D.; Hwang, S. H.; Zhou, Y.; Guan, C. X.; Liu, S. K.; Zhang, J. PTUPB Ameliorates High-Fat Diet-Induced Non-Alcoholic Fatty Liver Disease via Inhibiting NLRP3 Inflammasome Activation in Mice. *Biochem. Biophys. Res. Commun.* **2020**, *523*, 1020–1026.

(18) Zhang, C. H.; Zheng, L.; Gui, L.; Lin, J. Y.; Zhu, Y. M.; Deng, W. S.; Luo, M. Soluble Epoxide Hydrolase Inhibition with T-TUCB Alleviates Liver Fibrosis and Portal Pressure in Carbon Tetrachloride-Induced Cirrhosis in Rats. *Clin. Res. Hepatol. Gastroenterol.* **2018**, *42*, 118–125.

(19) Harris, T. R.; Bettaieb, A.; Kodani, S.; Dong, H.; Myers, R.; Chiamvimonvat, N.; Haj, F. G.; Hammock, B. D. Inhibition of Soluble Epoxide Hydrolase Attenuates Hepatic Fibrosis and Endoplasmic Reticulum Stress Induced by Carbon Tetrachloride in Mice. *Toxicol. Appl. Pharmacol.* **2015**, *286*, 102–111.

(20) Bettaieb, A.; Nagata, N.; AbouBechara, D.; Chahed, S.; Morisseau, C.; Hammock, B. D.; Haj, F. G. Soluble Epoxide Hydrolase Deficiency or Inhibition Attenuates Diet-Induced Endoplasmic Reticulum Stress in Liver and Adipose Tissue. *J. Biol. Chem.* **2013**, *288*, 14189–14199.

(21) Spector, A. A.; Fang, X.; Snyder, G. D.; Weintraub, N. L. Epoxyeicosatrienoic Acids (EETs): Metabolism and Biochemical Function. *Prog. Lipid Res.* **2004**, *43*, 55–90.

(22) Arvind, A.; Osganian, S. A.; Sjoquist, J. A.; Corey, K. E.; Simon, T. G. Epoxygenase-Derived Epoxyeicosatrienoic Acid Mediators Are Associated With Nonalcoholic Fatty Liver Disease, Nonalcoholic Steatohepatitis, and Fibrosis. *Gastroenterology* **2020**, *159*, 2232–2234e4.

(23) Raffaele, M.; Bellner, L.; Singh, S. P.; Favero, G.; Rezzani, R.; Rodella, L. F.; Falck, J. R.; Abraham, N. G.; Vanella, L. Epoxyeicosatrienoic Intervention Improves NAFLD in Leptin Receptor Deficient Mice by an Increase in PGC1 α -HO-1-PGC1 α -Mitochondrial Signaling. *Exp. Cell Res.* **2019**, *380*, 180–187.

(24) Wang, X.; Li, L.; Wang, H.; Xiao, F.; Ning, Q. Epoxyeicosatrienoic Acids Alleviate Methionine-Choline-Deficient Diet-Induced Non-Alcoholic Steatohepatitis in Mice. *Scand. J. Immunol.* **2019**, *90*, No. e12791.

(25) Liu, Y.; Dang, H.; Li, D.; Pang, W.; Hammock, B. D.; Zhu, Y. Inhibition of Soluble Epoxide Hydrolase Attenuates High-Fat-Diet-

Induced Hepatic Steatosis by Reduced Systemic Inflammatory Status in Mice. *PLoS One* **2012**, *7*, No. e39165.

(26) Schuck, R. N.; Zha, W.; Edin, M. L.; Gruzdev, A.; Vendrov, K. C.; Miller, T. M.; Xu, Z.; Lih, F. B.; DeGraff, L. M.; Tomer, K. B.; Jones, H. M.; Makowski, L.; Huang, L.; Poloyac, S. M.; Zeldin, D. C.; Lee, C. R. The Cytochrome P450 Epoxygenase Pathway Regulates the Hepatic Inflammatory Response in Fatty Liver Disease. *PLoS One* **2014**, *9*, No. e110162.

(27) Hye Khan, M. A.; Schmidt, J.; Stavniichuk, A.; Imig, J. D.; Merk, D. A Dual Farnesoid X Receptor/Soluble Epoxide Hydrolase Modulator Treats Non-Alcoholic Steatohepatitis in Mice. *Biochem. Pharmacol.* **2019**, *166*, 212–221.

(28) Helmstädter, M.; Schmidt, J.; Kaiser, A.; Weizel, L.; Proschak, E.; Merk, D. Differential Therapeutic Effects of FXR Activation, SEH Inhibition, and Dual FXR/SEH Modulation in NASH in Diet-Induced Obese Mice. *ACS Pharmacol. Transl. Sci.* **2021**, 966–979.

(29) Wu, F. P.; Peng, J. B.; Qi, X.; Wu, X. F. Palladium-Catalyzed Carbonylative Transformation of Organic Halides with Formic Acid as the Coupling Partner and CO Source: Synthesis of Carboxylic Acids. *J. Org. Chem.* **2017**, *82*, 9710–9714.

(30) Schmidt, J.; Klingler, F.-M.; Proschak, E.; Steinhilber, D.; Schubert-Zsilavecz, M.; Merk, D. NSAIDs Ibuprofen, Indometacin, and Diclofenac Do Not Interact with Farnesoid X Receptor. *Sci. Rep.* **2015**, *5*, No. 14782.

(31) Blöcher, R.; Lamers, C.; Wittmann, S. K.; Merk, D.; Hartmann, M.; Weizel, L.; Diehl, O.; Brüggerhoff, A.; Boß, M.; Kaiser, A.; Schader, T.; Göbel, T.; Grundmann, M.; Angioni, C.; Heering, J.; Geisslinger, G.; Wurglics, M.; Kostenis, E.; Brüne, B.; Steinhilber, D.; Schubert-Zsilavecz, M.; Kahnt, A.; Proschak, E. N-Benzylbenzamidates: A Novel Merged Scaffold for Orally Available Dual Soluble Epoxide Hydrolase/Peroxisome Proliferator-Activated Receptor γ Modulators. *J. Med. Chem.* **2016**, *59*, 61–81.

(32) Jones, P. D.; Wolf, N. M.; Morisseau, C.; Whetstone, P.; Hock, B.; Hammock, B. D. Fluorescent Substrates for Soluble Epoxide Hydrolase and Application to Inhibition Studies. *Anal. Biochem.* **2005**, *343*, 66–75.

(33) Obach, R. S. Prediction of Human Clearance of Twenty-Nine Drugs from Hepatic Microsomal Intrinsic Clearance Data: An Examination of In Vitro Half-Life Approach and Nonspecific Binding to Microsomes. *Drug Metab. Dispos.* **1999**, *27*, 1350–1359.

(34) Brian Houston, J. Utility of in Vitro Drug Metabolism Data in Predicting in Vivo Metabolic Clearance. *Biochem. Pharmacol.* **1994**, *47*, 1469–1479.

(35) Westphal, M. V.; Wolfstädter, B. T.; Plancher, J.-M.; Gatfield, J.; Carreira, E. M. Evaluation of Tert-Butyl Isosteres: Case Studies of Physicochemical and Pharmacokinetic Properties, Efficacies, and Activities. *ChemMedChem* **2015**, *10*, 461–469.

(36) Barnes-Seeman, D.; Jain, M.; Bell, L.; Ferreira, S.; Cohen, S.; Chen, X. H.; Amin, J.; Snodgrass, B.; Hatsis, P. Metabolically Stable Tert-Butyl Replacement. *ACS Med. Chem. Lett.* **2013**, *4*, 514–516.

(37) Sowaileh, M. F.; Hazlitt, R. A.; Colby, D. A. Application of the Pentafluorosulfanyl Group as a Bioisosteric Replacement. *ChemMedChem* **2017**, *12*, 1481–1490.

(38) Kulinkovich, O. G. The Chemistry of Cyclopropanols. *Chem. Rev.* **2003**, *103* (103), 2597–2632.

(39) Merk, D.; Lamers, C.; Ahmad, K.; Carrasco Gomez, R.; Schneider, G.; Steinhilber, D.; Schubert-Zsilavecz, M. Extending the Structure-Activity Relationship of Anthranilic Acid Derivatives as Farnesoid x Receptor Modulators: Development of a Highly Potent Partial Farnesoid x Receptor Agonist. *J. Med. Chem.* **2014**, *57*, 8035–8055.

(40) Merk, D.; Sreeramulu, S.; Kudlinzki, D.; Saxena, K.; Linhard, V.; Gande, S. L.; Hiller, F.; Lamers, C.; Nilsson, E.; Aagaard, A.; Wissler, L.; Dekker, N.; Bamberg, K.; Schubert-Zsilavecz, M.; Schwalbe, H. Molecular Tuning of Farnesoid X Receptor Partial Agonism. *Nat. Commun.* **2019**, *10*, No. 2915.

(41) Schierle, S.; Schmidt, J.; Kaiser, A.; Merk, D. Selective Optimization of Pramlintide to Farnesoid X Receptor Modulators. *ChemMedChem* **2018**, *13*, 2530–2545.

(42) Heitel, P.; Faudone, G.; Helmstädter, M.; Schmidt, J.; Kaiser, A.; Tjaden, A.; Schröder, M.; Müller, S.; Schierle, S.; Pollinger, J.; Merk, D. A Triple Farnesoid X Receptor and Peroxisome Proliferator-Activated Receptor α/δ Activator Reverses Hepatic Fibrosis in Diet-Induced NASH in Mice. *Commun. Chem.* **2020**, *3*, No. 174.

(43) Helmstädter, M.; Vietor, J.; Sommer, J.; Schierle, S.; Willems, S.; Kaiser, A.; Schmidt, J.; Merk, D. A New FXR Ligand Chemotype with Agonist/Antagonist Switch. *ACS Med. Chem. Lett.* **2021**, *12*, 267–274.

(44) Steri, R.; Achenbach, J.; Steinhilber, D.; Schubert-Zsilavecz, M.; Proschak, E. Investigation of Imatinib and Other Approved Drugs as Starting Points for Antidiabetic Drug Discovery with FXR Modulating Activity. *Biochem. Pharmacol.* **2012**, *83*, 1674–1681.

(45) Seuter, S.; Väisänen, S.; Rådmark, O.; Carlberg, C.; Steinhilber, D. Functional Characterization of Vitamin D Responding Regions in the Human 5-Lipoxygenase Gene. *Biochim. Biophys. Acta, Mol. Cell Biol. Lipids* **2007**, *1771*, 864–872.

(46) Wolf, N. M.; Morisseau, C.; Jones, P. D.; Hock, B.; Hammock, B. D. Development of a High-Throughput Screen for Soluble Epoxide Hydrolase Inhibition. *Anal. Biochem.* **2006**, *355*, 71–80.

(47) Heitel, P.; Achenbach, J.; Moser, D.; Proschak, E.; Merk, D. DrugBank Screening Revealed Alitretinoin and Bexarotene as Liver X Receptor Modulators. *Bioorg. Med. Chem. Lett.* **2017**, *27*, 1193–1198.

(48) Flesch, D.; Cheung, S.-Y.; Schmidt, J.; Gabler, M.; Heitel, P.; Kramer, J. S.; Kaiser, A.; Hartmann, M.; Lindner, M.; Lüddens-Dämgen, K.; Heering, J.; Lamers, C.; Lüddens, H.; Wurglics, M.; Proschak, E.; Schubert-Zsilavecz, M.; Merk, D. Non-Acidic Farnesoid X Receptor Modulators. *J. Med. Chem.* **2017**, *60*, 7199–7205.

(49) Gellrich, L.; Heitel, P.; Heering, J.; Kilu, W.; Pollinger, J.; Goebel, T.; Kahnt, A.; Arifi, S.; Pogoda, W.; Paulke, A.; Steinhilber, D.; Proschak, E.; Wurglics, M.; Schubert-Zsilavecz, M.; Chaikwad, A.; Knapp, S.; Bischoff, I.; Fürst, R.; Merk, D. L-Thyroxine and the Nonclassical Thyroid Hormone TETRAC Are Potent Activators of PPAR γ . *J. Med. Chem.* **2020**, *63*, 6727–6740.

(50) Rau, O.; Wurglics, M.; Paulke, A.; Zitzkowski, J.; Meindl, N.; Bock, A.; Dingermann, T.; Abdel-Tawab, M.; Schubert-Zsilavecz, M. Carnosic Acid and Carnosol, Phenolic Diterpene Compounds of the Labiate Herbs Rosemary and Sage, Are Activators of the Human Peroxisome Proliferator-Activated Receptor Gamma. *Planta Med.* **2006**, *72*, 881–887.

(51) Heitel, P.; Gellrich, L.; Kalinowsky, L.; Heering, J.; Kaiser, A.; Ohrndorf, J.; Proschak, E.; Merk, D. Computer-Assisted Discovery and Structural Optimization of a Novel Retinoid X Receptor Agonist Chemotype. *ACS Med. Chem. Lett.* **2019**, *10*, 203–208.